Structural Changes from the Pure Components to Nylon 6−Montmorillonite Nanocomposites Observed by Solid-State NMR

Marko Bertmer,*,† Mingfei Wang,† Mirko Krüger,† Bernhard Blümich,†
Victor M. Litvinov,‡ and Martin van Es§

Institute of Technical and Macromolecular Chemistry, Worringer Weg 1, 52056 Aachen, Germany, DSM Research, P. O. Box 18, 6160 MD Geleen, The Netherlands, and DSM Dyneema BV, R&D, P. O. Box 1163, 6160 BD Geleen, The Netherlands

Received December 19, 2005. Revised Manuscript Received December 9, 2006

Multinuclear solid-state NMR was used to characterize the molecular structures in nylon 6−montmorillonite nanocomposites in comparison with the two pure components. Both the polymer and the clay were studied. ^{27}Al two-dimensional multiple quantum magic angle spinning (MQMAS) measurements reveal the existence of an additional four-coordinated aluminum site in the nanocomposites compared to in the pure clay. This site is most probably induced by interactions of the polymer chains with the silicate surface. A highly mobile component is observed only in the ^{1}H NMR spectra of all nanocomposite samples, whose relative content increases with increasing clay content and which is generated during the extrusion process. High-resolution ^{1}H and ^{13}C NMR spectra of these mobile molecules are recorded and assigned to be a tertiary amine that is formed during the melt extrusion process as a result of the loss of one methyl group of the organic modifier dimethyl di(hydrogenated tallow) ammonium ion. As a result of the presence of paramagnetic Fe^{3+} inside the clay, the proton spin−lattice relaxation time of the polymer is strongly influenced. This effect can be used to get information on the degree of clay exfoliation. It was found that at higher clay contents on average just two platelets are stuck together. With this, the distance between clay platelets is calculated and correlated with the analysis of TEM (transmission electron microscopy) measurements. ^{15}N cross-polarization magic angle spinning (CPMAS) spectra show an increase of the fraction of the γ-crystalline phase at the cost of the α-crystalline phase upon increasing clay content.

1. Introduction

Nanocomposites from polymers and layered silicates exhibit excellent mechanical and thermal properties that cannot be obtained from the pure components or a microscopic mixture of the two components.[1] This makes these compounds interesting for both scientific and commercial reasons. A variety of procedures for obtaining nanocomposites from various polymers together with different organically modified layered silicates have been developed.[1−18]

Routinely, X-ray and transmission electron microscopy (TEM) measurements are employed to characterize the quality of exfoliation of the silicate platelets in these nanocomposites.[1] The use of solid-state NMR to characterize polymer-layered silicate nanocomposites has recently increased significantly. Mainly ^{1}H T_1 relaxation studies[19−22] and ^{13}C cross-polarization magic angle spinning (CPMAS) measurements[20,23−27] have been used for this purpose.

* Corresponding author. E-mail: mbertmer@mc.rwth-aachen.de.
† Institute of Technical and Macromolecular Chemistry.
‡ DSM Research.
§ DSM Dyneema BV, R&D.

(1) Alexandre, M.; Dubois, P. *Mater. Sci. Eng.* **2000**, *28*, 1−63.
(2) Vaia, R. A.; Vasudevan, S.; Krawiec, W.; Scanlon, L. G.; Giannelis, E. P. *Adv. Mater.* **1995**, *7*, 154−156.
(3) Burnside, S. D.; Giannelis, E. P. *Chem. Mater.* **1995**, *7*, 1597−1600.
(4) Giannelis, E. P. *Adv. Mater.* **1996**, *8*, 29−35.
(5) Liu, L.; Qi, Z.; Zhu, X. *J. Appl. Polym. Sci.* **1998**, *71*, 1133−1138.
(6) Ke, Y.; Long, C.; Qui, Z. *J. Appl. Polym. Sci.* **1998**, *71*, 1139−1146.
(7) Zhang, L.; Wang, Y.; Wang, Y.; Sui, Y.; Yu, D. *J. Appl. Polym. Sci.* 2000, *78*, 1873−1878.
(8) Ma, J.; Qi, Z.; Hu, Y. *J. Appl. Polym. Sci.* **2001**, *82*, 3611−3617.
(9) Wu, Z.; Zhou, C.; Qi, R.; Zhang, H. *J. Appl. Polym. Sci.* **2001**, *83*, 2403−2410.
(10) Tseng, C. R.; Wu, J. Y.; Lee, H. Y.; Chang, F. C. *J. Appl. Polym. Sci.* **2001**, *85*, 1370−1377.
(11) Alexandre, M.; Beyer, G.; Henrist, C.; Cloots, R.; Rulmont, A.; Jérôme, R.; Dubois, P. *Chem. Mater.* **2001**, *13*, 3830−3832.
(12) Yeh, J.-M.; Liou, S.-J.; Lin, C.-Y.; Cheng, C.-Y.; Chang, Y.-W. *Chem. Mater.* **2002**, *14*, 154−161.
(13) Lim, S. K.; Kim, J. W.; Chin, I.; Kwon, Y. K.; Choi, H. J. *Chem. Mater.* **2002**, *14*, 1989−1994.
(14) Wang, D.; Zhu, J.; Yao, Q.; Wilkie, C. A. *Chem. Mater.* **2001**, *14*, 3837−3843.
(15) Triantafillidis, C. S.; LeBaron, P. C.; Pinnavaia, T. J. *Chem. Mater.* **2002**, *14*, 4088−4095.
(16) Maiti, P.; Yamada, K.; Okamoto, M.; Ueda, K.; Okamoto, K. *Chem. Mater.* **2002**, *14*, 4654−4661.
(17) Wang, S.; Hu, Y.; Tang, Y.; Wang, Z.; Chen, Z.; Fan, W. *J. Appl. Polym. Sci.* **2002**, *89*, 2583−2585.
(18) Artzi, N.; Nir, Y.; Narkis, M.; Siegmann, A. *J. Polym. Sci., Part B* **2002**, *40*, 1741−1753.
(19) VanderHart, D. L.; Asano, A.; Gilman, J. W. *Chem. Mater.* **2001**, *13*, 3796−3809.
(20) VanderHart, D. L.; Asano, A.; Gilman, J. W. *Macromolecules* **2001**, *34*, 3819−3822.
(21) Bourbigot, S.; Vanderhart, D. L.; Gilman, J. W.; Awad, W. H.; Davis, R. D.; Morgan, A. B.; Wilkie, C. A. *J. Polym. Sci., Part B* **2003**, *41*, 3188−3213.
(22) Calberg, C.; Jérôme, R.; Grandjean, J. *Langmuir* **2004**, *20*, 2039−2041.
(23) Forte, C.; Geppi, M.; Giamberini, S.; Ruggeri, G.; Veracini, C. A.; Mendez, B. *Polymer* **1998**, *39*, 2651−2656.
(24) Harris, D. J.; Bonagamba, T. J.; Schmidt-Rohr, K. *Macromolecules* **1999**, *32*, 6718−6724.
(25) VanderHart, D. L.; Asano, A.; Gilman, J. W. *Chem. Mater.* **2001**, *13*, 3781−3795.
(26) Sahoo, S. K.; Kim, D. W.; Kumar, J.; Blumstein, A.; Cholli, A. L. *Macromolecules* **2003**, *36*, 2777−2784.

10.1021/cm052798x CCC: $37.00
Published on Web 02/02/2007

VanderHart et al. developed a strategy to determine the quality of clay dispersion from ^{1}H NMR relaxation measurements in clays with paramagnetic impurities.[21,28] ^{29}Si NMR heteronuclear correlation spectra were employed by Schmidt-Rohr et al.[29−31] to obtain information about the polymer chain fragment adjacent to the clay surface in nanocomposites with hectorite clay. Furthermore, it was demonstrated by Mathias et al.[32] that different crystalline polymorphs in nylon 6−montmorillonite nanocomposites can be characterized by measuring ^{15}N CPMAS NMR spectra.

The amount of clay was relatively low (up to 5 wt %) in previous studies of nanocomposites. In the present study, a much wider range of compositions is used to gain a better understanding of the effect of clay content on molecular structure. Samples prepared with a clay content of up to 20 wt % still show very good clay exfoliation. This enables the study of the clay structure by ^{27}Al Bloch decay spectra and two-dimensional (2D) multiple-quantum magic angle spinning (MQMAS)[33] measurements. The effect of paramagnetic Fe^{3+} ions on the ^{1}H T_1 relaxation time of the polymer is used to study the degree of clay exfoliation. Furthermore, a comparison with the silicate platelet distance calculated from composition for perfect exfoliation and from the analysis of TEM images is attempted. Finally, to get detailed information about the highly mobile molecules in the nanocomposites, rotor-synchronized Hahn echo ^{1}H and ^{13}C NMR spectra are recorded.

2. Experimental Section

2.1. Samples. A series of nylon 6−montmorillonite nanocomposites with clay contents between 0 and 20 wt % was prepared at DSM Geleen.[34] The trade name of nylon 6 is Akulon 123 with a number average molecular weight of 13 000 g mol^{-1} and a weight average molecular weight of 24 000 g mol^{-1}. The clay is montmorillonite where the Na^+ counterions were exchanged by dimethyl di(hydrogenated tallow) ammonium ions. The clay was provided by Southern Clay Products, TX (Cloisite 20A). The organic content of the clay was 38.1 wt % whereas 32 wt % would be sufficient for charge compensation. The additional surfactant is used to obtain a better and faster exfoliation.

A master batch was produced from 66.6 wt % nylon 6 and 33.4 wt % Cloisite 20A. The dry blended mixture was fed into a corotating twin screw extruder (W&P ZSK 30 42D) which was operated at 400 rpm. The setup of the extruder comprises a melting part, a contra-rotating part, an injection gate for water, a second contra-rotating part, and a degassing part for removing the water. The water is used to allow extrusion at temperatures between 190 and 215 °C over the entire length of the cylinder which is below the melting temperature of dry nylon 6. The dry clay/nylon mixture was continuously fed to the extruder at a throughput of 4 kg/h. Water was injected into the melt at a throughput of 20 g/min (which corresponds to about 30% by weight of water, relative to the nylon 6) and discharged via the degassing gate at the end of the extruder at a pressure varying from 3 to 6 kPa. The presence of water considerably lowers the melting temperature of nylon 6. A big benefit of the low temperature is that it prevents degradation of the polymer and the clay modification. The polyamide nanocomposite composition was extruded as a strand which was cooled in water.[35]

Table 1. Composition of Nylon 6−Montmorillonite Nanocomposites[a]

sample	silicate	clay modifier	nylon 6
PA(0)	0.00	0.00	100.00
PA(0.2)	0.20	0.13	99.67
PA(1)	1.00	0.67	98.33
PA(2.5)	2.50	1.68	95.83
PA(5)	5.00	3.35	91.65
PA(7.5)	7.50	5.03	87.48
PA(10)	10.00	6.70	83.30
PA(15)	15.00	10.05	74.95
PA(20)	20.00	13.40	66.60

[a] Values are given in wt %.[34]

Individual samples were prepared by diluting the master batch with nylon 6 using the same extruder. Table 1 shows the relative content of polymer, clay, and organic modifier. The notation of samples is PA(x) where x denotes the amount of clay in wt %.

2.2. TEM Measurements. TEM pictures were taken with a Phillips CM200 at an acceleration voltage of 120 kV.[34] The samples were first embedded in an epoxy resin. Afterward, films with a thickness of about 70 nm were microtomed using liquid nitrogen for cooling.

2.3. NMR Measurements. All NMR experiments were performed on a Bruker Avance DSX 500 spectrometer with a ^{1}H frequency of 500.46 MHz. The frequencies of the other nuclei are determined by their gyromagnetic ratios relative to the ^{1}H frequency. For the ^{1}H, ^{13}C, and ^{27}Al measurements a 4 mm MAS probe and for the ^{15}N spectra a 7 mm MAS probe were used. The chemical shifts were referenced to tetramethylsilane (TMS) for ^{1}H and ^{13}C measurements. The reference for ^{27}Al was an aqueous 1 M solution of $Al(NO_3)_3$. Finally, the shifts in the ^{15}N spectra were referenced to nitromethane using glycine as a secondary reference. It is mentioned that our chemical shift values differ from those of Mathias et al.[32] because they used glycine as reference sample (= 0 ppm) whereas we used the officially recommended reference nitromethane by using glycine as a secondary reference with a chemical shift of −347 ppm. No special treatment of the samples prior to the NMR measurements was done.

2.3.1. ^{1}H T_1 Measurements. To measure the T_1 of the protons from nylon 6 only, we used the saturation-recovery pulse sequence followed by cross-polarization to ^{13}C. The cross-polarization time was 1 ms. The relaxation of the highly mobile molecules, which, shown below, are present in the nanocomposites, is not detected by this experiment because of their low cross-polarization efficiency. The spin−lattice relaxation time of protons close to the clay surface is reduced by the Fe^{3+} ions of the clay. Furthermore, by proton spin diffusion this effect propagates to the more distant protons. T_1 values were obtained from single-exponential fits. In general, the analysis is more complicated because of the complex morphology of nylon 6 and the influence of paramagnetic iron. For more detailed information the reader is referred to the literature.[19]

(27) Hrobarikova, J.; Robert, J.-L.; Calberg, C.; Jérôme, R.; Grandjean, J. *Langmuir* **2004**, *20*, 9828−9833.
(28) Gilman, J. W.; Bourbigot, S.; Shields, J. R.; Nyden, M.; Kashigawi, T.; Davis, R. D.; VanderHart, D. L.; Demory, W.; Wilkie, C. A.; Morgan, A. B.; Harris, J.; Lyon, R. E. *J. Mater. Sci.* **2003**, *38*, 4451−4460.
(29) Hou, S. S.; Beyer, F. L.; Schmidt-Rohr, K. *Solid State Nucl. Magn. Reson.* **2002**, *22*, 110−127.
(30) Hou, S.-S.; Schmidt-Rohr, K. *Chem. Mater.* **2003**, *15*, 1938−1940.
(31) Hou, S.-S.; Bonagamba, T. J.; Beyer, F. L.; Madison, P. H.; Schmidt-Rohr, K. *Macromolecules* **2003**, *36*, 2769−2776.
(32) Mathias, L. J.; Davis, R. D.; Jarrett, W. L. *Macromolecules* **1999**, *32*, 7958−7960.
(33) Medek, A.; Harwood, J. S.; Frydman, L. *J. Am. Chem. Soc.* **1995**, *117*, 12779−87.
(34) van Es, M. Polymer-Clay Nanocomposites - The importance of particle dimensions. Ph.D. thesis, Technische Universiteit Delft, Delft, 2001.
(35) Korbee, R. Patent Appl. WO 99/29767 DSM, 1999.

2.3.2. ^{15}N Measurements. ^{15}N CPMAS spectra were obtained using a cross-polarization time of 1 ms and a magic angle spinning speed of 5 kHz. For all the samples studied, the same measuring parameters, that is, spinning speed and contact time, have been employed. With this and the fact that the contact time behavior is the same in all samples, a comparison between different samples is possible, although cross-polarization in general is not a quantitative technique. Because of the different contact time behaviors of the amorphous and crystalline phases the absolute phase composition is not reflected correctly. From X-ray diffraction techniques as well as ^1H T_2 measurements[34] the crystallinity in the nanocomposite samples varies between 50 and 60%. However, we only compare the relative contents of the α- and γ-crystalline phases.

Deconvolution of ^{15}N CPMAS spectra was performed using the program dmfit.[36] The ^{15}N chemical shifts of signals of the α-crystalline, the γ-crystalline, and the amorphous phases are −263 ppm, −258 ppm, and −259.5 ppm, respectively.

2.3.3. ^1H and ^{13}C Spectra of the Highly Mobile Component. To obtain spectra solely of the highly mobile molecules (see below), a rotor-synchronized Hahn echo experiment was performed at a spinning speed of 10 kHz with a total echo time of 4 ms for ^1H and 2 ms for ^{13}C, respectively, and a recycle delay of 5 s. In the case of the ^{13}C NMR measurement, direct excitation instead of cross-polarization was done together with ^1H decoupling during acquisition. The magnetization of the strongly coupled nuclei dephases during the echo time and only that of the highly mobile molecules is refocused, yielding spectra without signals from the rigid components and therefore allowing for better resolution.

2.3.4. ^{27}Al Measurements. Bloch decay spectra were recorded with a pulse width of 0.3 μs corresponding to a flip angle of less than 10°, fast repetition time of 30 ms, and spectral window of 2.5 MHz. The spinning speed was set to 15 kHz to prevent signal overlap with spinning sidebands.

In the 2D MQMAS experiment[33] a correlation between the standard MAS spectrum in the direct dimension and the isotropic spectrum in the indirect dimension is obtained. The modified sequence from Amoureux et al.[37] was employed that uses two high-power pulses to excite triple quantum coherence and reconvert it back to zero quantum coherence. After a z-filter time of 1 ms, readout is done with a low-power pulse that selectively excites the central transition. Pulse lengths were 3 and 1 μs for the two high-power pulses and 7.3 μs for the low-power pulse. Pure absorption 2D spectra were obtained with the States method.[38] A shearing transformation has to be done to obtain a purely isotropic frequency component along the F_1 axis. The t_1 increment was 5 μs. In order to obtain a higher signal-to-noise ratio the experiment was not performed rotor-synchronized in the F_1 dimension because of rapid signal decay. This results in spinning sidebands in the F_1 dimension.

In the standard one-pulse spectrum of a quadrupolar nucleus the chemical shift is different from the isotropic chemical shift because of the quadrupolar induced shift.[39] In the 2D MQMAS experiment these two contributions can be separated. From the position of the signals in both dimensions the isotropic chemical shift and the second-order quadrupolar effect (SOQE) can be calculated.[39] The latter is defined as

$$\mathrm{SOQE} = C_q\sqrt{1+\frac{\eta^2}{3}} \quad (1)$$

where C_q is the quadrupolar coupling and η is the asymmetry parameter. Because of this, C_q and η cannot be evaluated separately which results in an uncertainty for the quadrupolar coupling constant of about 10−15%.

3. Results

3.1. Quality of Exfoliation from TEM Data. TEM measurements are routinely used for nanocomposites to check for intercalated or exfoliated clay platelets as well as for their orientation. TEM pictures were taken for all samples. Good clay exfoliation of nylon 6−montmorillonite nanocomposites can be seen in Figure 1 for samples with 1, 5, and 15 wt % of clay. The length of the clay layers is about 100 nm. With the thickness of a clay platelet of about 1 nm, the aspect ratio is 100.

At 1 wt % clay content the exfoliation is almost perfect. With a clay loading of 5 wt %, some platelets are fully exfoliated while the majority of clay exists in groups consisting of two platelets still stuck together. However, those groups are very well dispersed in the polymer matrix. At 15 wt % clay loading the groups of two platelets are highly oriented and form large aggregates. Platelets and groups of two platelets are mainly oriented along the plane of the sheet, that is, along the flow direction during the injection molding process. For the 1 wt % sample, the orientation of platelets is not perfect, while for the 15 wt % sample, the orientation inside the aggregates is very good; however, the orientation of these aggregates with respect to each other is random.

An attempt was made to determine the platelet distance from TEM data ($\overline{D_{TEM}}$) by using the following procedure.[34] A line is drawn perpendicular to the orientation direction—and with that the plane of the platelets—in the TEM image. Then, for the fractional length f_L of that line drawn in the plane, the following equation holds

$$f_L = \frac{nd}{L} \quad (2)$$

n is the number of intersecting clay platelets seen in the TEM image, d is the thickness of a single clay platelet (1 nm), and L is the total length of the drawn line. It should be mentioned that the equation is only valid in the case of perfect orientation and if the line is drawn perpendicular to the orientation direction. It can be shown[40] that the fractional length f_L is equal to the volume fraction f_V. Accordingly, the distance between platelets can be calculated

$$\overline{D_{TEM}} = \frac{L-nd}{n} \quad (3)$$

Table 2 summarizes the clay platelet distances obtained in this way. In the next section we want to compare these results with those derived from ^1H T_1 relaxation data.

(36) Massiot, D.; Fayon, F.; Capron, M.; King, I.; Calvé, S. L.; Alonso, B.; Durand, J.-O.; Bujoli, B.; Gan, Z.; Hoatson, G. *Magn. Reson. Chem.* **2002**, *40*, 70−76.
(37) Amoureux, J. P.; Fernandez, C.; Steuernagel, S. *J. Magn. Reson., Ser. A* **1996**, *123*, 116−23.
(38) States, D. J.; Haberkorn, R. A.; Ruben, D. J. *J. Magn. Reson.* **1982**, *48*, 286−92.
(39) Fernandez, C.; Amoureux, J. P.; Chezeau, J. M.; Delmotte, L.; Kessler, H. *Microporous Mater.* **1996**, *6*, 331−40.
(40) Kämpf, G. *Characterization of Plastics by Physical Methods; Experimental Techniques and Practical Applications;* Hanser: München, 1986.

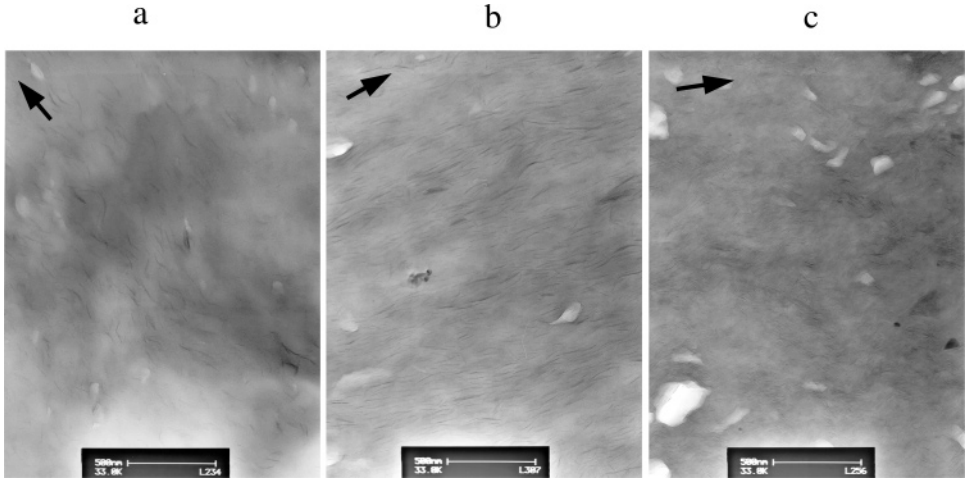

Figure 1. TEM images of nylon 6−montmorillonite nanocomposites with 1 (a), 5 (b), and 15 wt % (c) silicate. The arrows indicate the orientation of the platelets.

Table 2. Inter-Platelet Distances $\overline{D}$ (in nm) As Determined from TEM Images[34] and Analysis of T_1 Data with the Use of Composition

sample	$\overline{D_{TEM}}$	$\overline{D_{T_1}}$	sample	$\overline{D_{TEM}}$	$\overline{D_{T_1}}$
PA(0.2)	1350	1250[a]	PA(7.5)	13	62
PA(1)	256	250[a]	PA(10)	15	44
PA(2.5)	71	202	PA(15)	7	26
PA(5)	25	97	PA(20)	4	18

[a] Value calculated directly from composition for the case of perfect exfoliation.

3.2. Effect of Paramagnetic Fe^{3+} Ions on the Proton Spin−Lattice Relaxation Time. Naturally occurring montmorillonite contains Fe^{3+} ions at a content between 2 and 5 wt %, replacing mainly the Al^{3+} ions in the octahedral position (for the description of the clay structure see below). The analysis of the clay Cloisite 20A yielded a wt % of Fe_2O_3 of 3.11% (analysis by Southern Clay, TX). This paramagnetic impurity strongly influences the spin−lattice relaxation time (T_1) of the nuclei, for example, protons, in the proximity of the clay surface and consecutively also the protons of nylon 6 further away by spin diffusion.[19] Therefore, the paramagnetic ions influence T_1 depending on the Fe^{3+} concentration in the clay, which is assumed to be constant in all samples, and on the mean distance between clay platelets, which is influenced by the sample composition and the clay exfoliation. A better exfoliation of the clay sheets results in a higher clay−polyamide interfacial area, smaller distance between clay layers that interact with the polymer, and therefore a shorter spin-diffusion path. The influence of the Fe^{3+} ions on the T_1 of the polymer is stronger in the case of full exfoliation; therefore, ^1H T_1 measurements can be used for the determination of the quality of clay dispersion, as has been shown by VanderHart in nanocomposites of montmorillonite with nylon 6[25] and polystyrene[21] using a spin-diffusion model. We will use a semiquantitative approach to visualize the correlation of the paramagnetic contribution to the spin−lattice relaxation rate with the clay dispersion.[20] A full spin-diffusion analysis was described by Vanderhart[21,25] and is outside the scope of this manuscript. Our goal is to obtain a semiquantitative picture of the clay dispersion as a function of clay content using certain assumptions for analysis, and, therefore, the resulting interplatelet distances (cf. Table 2) should not be understood as absolute values but will help in showing the trend of clay dispersion.

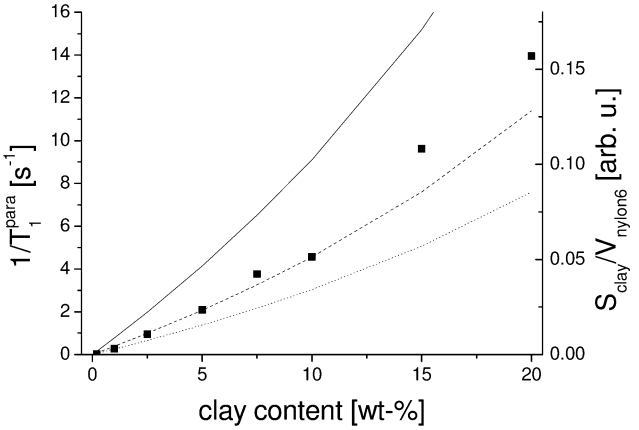

Figure 2. Spin−lattice relaxation rate and surface-to-volume ratio as a function of clay content. Data points refer to the determined T_1^{para}, and the lines refer to the surface-to-volume ratios in the case of perfect exfoliation (solid line) and of two (dashed line) and three platelets (dotted line) stuck together, respectively.

Figure 2 displays the paramagnetic contribution to the ^1H spin−lattice relaxation rate ($1/T_1^{para}$) as a function of clay content. The strong influence of the paramagnetic Fe^{3+} is clearly visible. The spin−lattice relaxation rate can be expressed as

$$\frac{1}{T_1} = \frac{1}{T_1^{nylon6}} + \frac{1}{T_1^{para}} \tag{4}$$

where T_1^{nylon6} is the spin−lattice relaxation of pure nylon 6 and T_1^{para} the contribution to the spin−lattice relaxation time of nylon 6 caused by the paramagnetic Fe^{3+} inside the clay. It has to be kept in mind that if large tactoids with layered clay platelets are present, their contribution to T_1^{para} will be smaller. This will finally lead to an underestimation of the quality of the clay dispersion in such a way that the derived platelet separation is higher than that in some parts of the sample.

The spin−lattice relaxation rate is proportional to the surface-to-volume ratio. This assumption derives from the

observation of this effect in solutions[41] where a direct correlation of paramagnetic content and relaxivity was found.

$$\frac{S_{\text{clay}}}{V_{\text{nylon6}}} \propto \frac{1}{T_1^{\text{para}}} \tag{5}$$

The surface-to-volume ratio can be calculated from the composition and the specific densities of 2.7, 1.0, and 1.13 g cm^{-3} for the clay, the organic modifier, and the nylon 6, respectively, together with clay dimensions of 1 nm thickness and 100 nm length. Three cases are included in Figure 2, that is, perfect exfoliation and groups of two and three platelets stuck together, respectively. Two or three platelets stuck together reduce the clay−polyamide interfacial area by factors of 2 and 3, respectively. However, correlation between relaxation rate and surface-to-volume ratio requires a sample with known clay dispersion. The sample with a clay content of 1 wt % showed in the TEM image almost perfect exfoliation. Nevertheless, at this low clay content a very large separation of clay layers is present which means that the paramagnetic contribution to the spin−lattice relaxation rate will be too small to be correlated with the results for higher clay contents. According to Vanderhart et al.[19] and with $T_1(^1H) = 1.63$ s it can be computed that spin diffusion will be effective at a distance of maximum 50 nm which is significantly smaller than the mean distance between clay platelets according to TEM (Table 2). Therefore, for samples PA(0.2) and PA(1) a correlation with T_1^{para} using eq 4 is not possible. According to TEM data it is assumed that these samples have almost perfect exfoliation. We used the samples with 2.5 and 5 wt % clay to establish a correlation of the effect of clay content on clay exfoliation at higher amounts of clay. These samples showed in the TEM images good exfoliation with an average of two clay platelets stuck together. This fact was used to get a proportionality constant for eq 5. Both the 2.5 and the 5 wt % sample give almost identical proportionality constants, and the average value of the two was used to get the correlations for the other clay contents.

It can be seen that for clay contents higher than 1 wt % a very good correlation of the data points with the line corresponding to two platelets stuck together exists. This demonstrates the reasonable good clay dispersion up to high clay contents in these samples.

Clearly, the higher the clay−nylon interfacial area for a given clay concentration, the smaller the separation of clay platelets ($\overline{D_{T_1}}$) within the polymer matrix.

$$S_{\text{clay}} \propto \frac{1}{\overline{D_{T_1}}} \tag{6}$$

With the specific densities together with the number of platelets stuck together as derived from the T_1 data the average clay platelet distances can be estimated. Again, the 2.5 and 5 wt % samples were used for scaling with the TEM data. The values are included in Table 2.

Comparing the results of TEM and NMR, it can be seen that the platelet separation derived from the TEM analysis is smaller than from the NMR analysis. Therefore, the TEM data pretend better clay exfoliation. This can be explained by the fact that the number of lines seen on a TEM image can appear to be higher than the amount of platelets in the sample. If clay platelets are not oriented directly parallel to the electron beam, due to Bragg reflexions multiple lines can result in the TEM image. Nevertheless, as shown by the TEM images, the exfoliation is not perfect which is also concluded from the T_1 analysis. Concerning the NMR data, large aggregates of clay platelets will not really contribute to T_1^{para}, and, therefore, NMR can underestimate the exfoliation degree. The result will be a larger platelet separation.

The TEM and NMR analyses use different assumptions and therefore the resulting platelet separation does not give a quantitative picture but indicates the trend of clay dispersion as a function of clay content. Furthermore, it has to be mentioned that NMR is a bulk method whereas TEM only yields data for a specific part of the sample that does not need to be representative for the whole sample. Therefore, the values in Table 2 should be understood as being indicative of the quality of clay dispersion and not as accurate numbers as can be concluded from different values determined by TEM and NMR. This analysis is semiquantitative but yields interesting information about the trend of clay dispersion as a function of clay content.

Summarizing, this semiquantitative approach for the correlation of TEM and T_1 data with clay dispersion gives reasonable data and demonstrates the good clay exfoliation even for high clay contents. Clearly, a full analysis using a spin-diffusion model could be more accurate, but our primary goal was to estimate the quality of clay exfoliation.

3.3. Influence of Clay on the Phase Composition of Nylon 6. Nylon 6 exhibits a complex phase composition consisting of an amorphous phase and α- and γ-crystalline phases. NMR spectroscopy can be used for the analysis of the phase composition. However, the individual resonances of crystalline and amorphous phases in ^{13}C CPMAS spectra overlap strongly. Separation of crystalline and amorphous phases is possible by different procedures[42−44] such as Bloch decay spectra with a short recycle delay and the CPT_1 technique of Torchia.[45] However, as a result of the rapid sample cooling (see Experimental Section) the ^{13}C spectral resolution is lower as in comparable studies[20,25] possibly because of less ordered crystalline phases. Therefore, we chose to use ^{15}N CPMAS measurements to deduce the relative amounts of the α- and the γ-crystalline phase. Mathias et al.[46] demonstrated the usefulness of ^{15}N CPMAS experiments for the analysis of the phase composition in nylon 6. In comparison to the ^{13}C NMR spectra only one resonance exists for each phase. Because of partial overlap of the signals, a deconvolution of the spectra is required

(41) Foley, I;, Farooqui, S. A.; Kleinberg, R. L. *J. Magn. Reson., Ser. A* **1996**, *123*, 95−104.

(42) VanderHart, D. L.; Peréz, E. *Macromolecules* **1986**, *19*, 1902−1909.
(43) Hatfield, G. R.; Glans, J. H.; Hammond, W. B. *Macromolecules* **1990**, *23*, 1654−1658.
(44) Schreiber, R.; Veeman, W. S.; Gabriëlse, W.; Arnauts, J. *Macromolecules* **1999**, *32*, 4647−57.
(45) Torchia, D. A. *J. Magn. Reson.* **1978**, *30*, 613−616.
(46) Powell, D. G.; Mathias, L. J. *J. Am. Chem. Soc.* **1990**, *112*, 669−675.

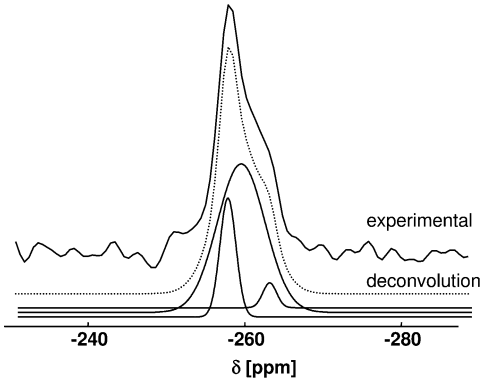

Figure 3. ^{15}N CPMAS spectrum of sample PA(5) (solid line) together with the simulated spectrum (dashed line). The three line shapes at the bottom (dotted lines) represent the individual line shapes of the γ-crystalline (−258.0 ppm), the α-crystalline (−263 ppm), and the amorphous (−259.5 ppm) phases, respectively.

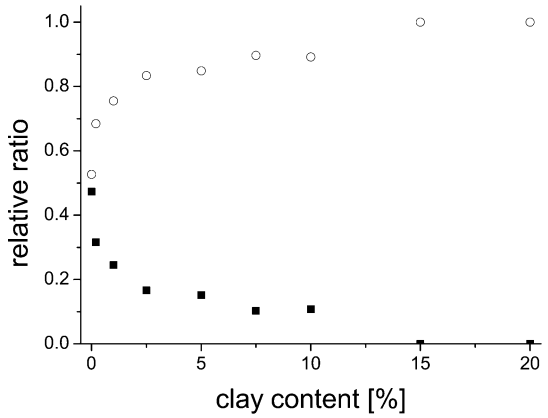

Figure 4. Relative content of the crystal fraction for α- (solid squares) and γ-crystalline phases (open circles) from ^{15}N CPMAS spectra as a function of clay content.

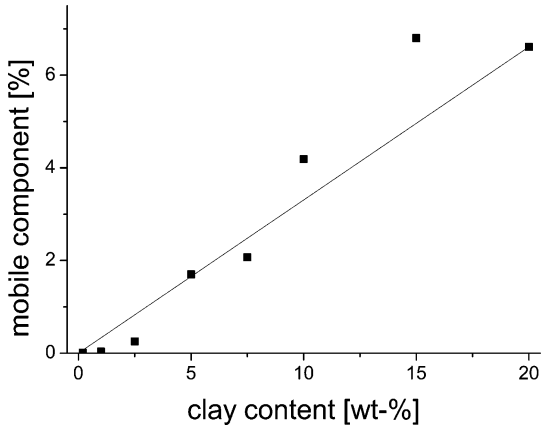

Figure 5. Relative fraction of the highly mobile component in the ^{1}H spectra as a function of clay content. The solid line is derived from the dilution of the master batch with 20 wt % clay.

which is fairly simple. As an example, Figure 3 shows the ^{15}N CPMAS spectrum of sample PA(5) together with the individual line shapes for the crystalline and amorphous phases. With the help of spectral deconvolution, the relative amounts of the different phases can be obtained. A plot of the relative content of α- and γ-crystalline phases as a function of clay content is shown in Figure 4. The amount of the γ-crystalline phase largely increases upon increasing the clay content from 0 wt % up to 2.5 wt % which is in agreement with results of previous studies that have been

Scheme 1. Structure of the Tertiary Amine[a]

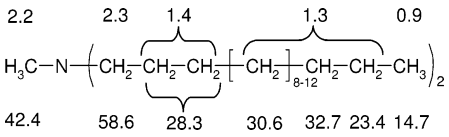

[a] ^{1}H and ^{13}C chemical shifts (in ppm) are printed above and below the structure, respectively.

performed for nylon 6 nanocomposites with low clay content.[47] The α to γ ratio is affected by the presence of clay[19,25,32] crystallization conditions and influences of clay particles on crystallization kinetics and shear flow. The amount of α- and γ-crystal polymorphs strongly depends on the crystallization conditions, such as the crystallization temperature, cooling rate, shear rate, humidity, and pressure. Crystallization of nylon 6 at temperatures below 130 °C and above 190 °C leads solely to the formation of γ- and α-crystals, respectively.[48−50] This effect of temperature is attributed to the crystallization rates for α- and γ -phases, namely, the formation of γ-crystals is faster below 130 °C, while above 190 °C it is faster for α-crystals.[50] Rapid cooling of nylon 6 melts favors γ-crystal formation.[51] Nylon 6 nanocomposites with low clay content contain large fractions of γ-crystals, which could be explained by fast cooling of the compounds after extrusion in water. Other studies have pointed out as well that the formation of the γ-crystalline phase in the nanocomposite is favored compared to the pure nylon 6[32,25,19,52,53] and increases during annealing for samples that were cooled slowly after extrusion.[32] At higher clay contents, the increase in γ-crystalline content is slowing, and at 15 and 20 wt % of clay no α-crystalline phase can be detected within the accuracy of the measurement.

On a similar system, VanderHart et al.[19] employed the possibility to differentiate α- and γ-crystalline phases by ^{13}C detection to separate their ^{1}H T_1 relaxation times. It was concluded that the γ-crystalline phase is preferentially closer to the clay surface than the α-crystalline phase. This coincides with our data because with increasing clay content the total clay-polyamide interfacial area increases, and with this the amount of γ-crystalline phase increases as well. It has been suggested that the clay surface initially favors the formation of γ-crystallites because protonated amino end groups of nylon 6 are ionically bound to the clay surface. This clay polymer interaction aligns the nylon 6 chains parallel to each other in the proper orientation for the formation of the γ-crystalline phase.[54] At high clay contents the exfoliation is not perfect; groups of two platelets are formed that decrease the accessibility of the clay surface.

(47) Lincoln, D. M.; Vaia, R. A.; Wang, Z.-G.; Hsiao, B. S.; Krishnamoorti, R. *Polymer* **2001**, *42*, 9975−9985.
(48) Illers, K. H.; Haberkorn, H. *Makromol. Chem.* **1971**, *142*, 31.
(49) Gurato, G.; Fichera, A.; Grandi, F. Z.; Zanetti, R.; Canal, P. *Makromol. Chem.* **1974**, *175*, 953.
(50) Kyotani, M.; Mitsuhashi, S. *J. Polym. Sci., Part A* **1972**, *10*, 1497.
(51) Murthy, N. S.; Aharoni, S. M.; Szollosi, A. B. *J. Polym. Sci., Polym. Phys.* **1985**, *23*, 2549.
(52) Devaux, E.; Bourbigot, S.; El Achari, A. *J. Appl. Polym. Sci.* **2002**, *86*, 2416−2423.
(53) Kojima, Y.; Usuki, A.; Kawasumi, M.; Okada, A.; Kurauchi, T.; Kamigaito, O.; Kaji, K. *J. Polym. Sci., Part B* **1994**, *32*, 625−630.
(54) Davis, R. D.; Jarrett, W. L.; Mathias, L. J. *ACS Symp. Ser.* **2002**, *804*, 117−126.

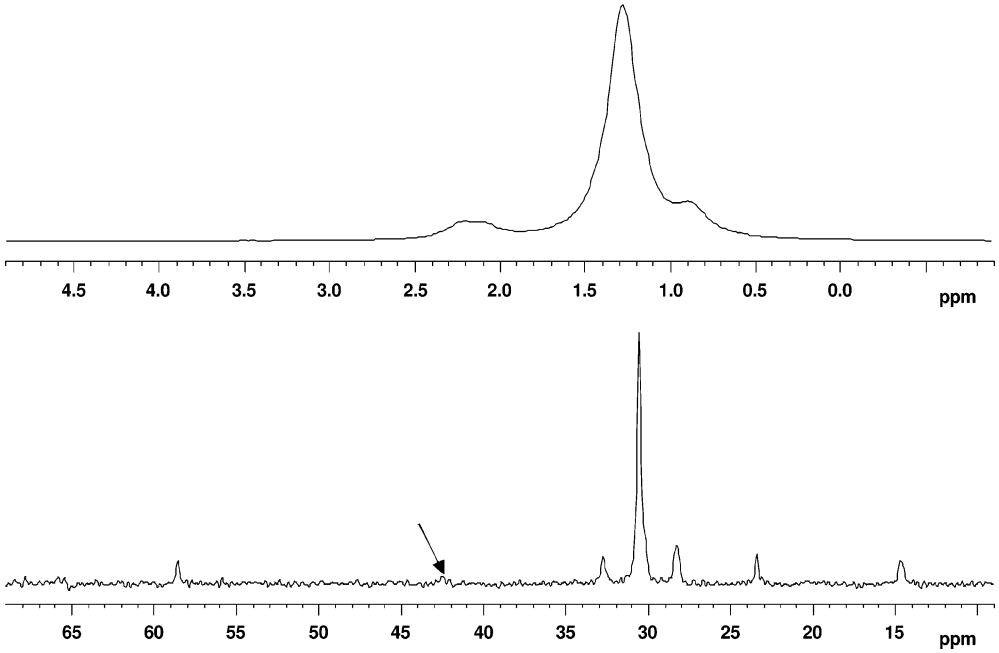

Figure 6. Rotor-synchronized ^{1}H (top) and ^{13}C (bottom) Hahn echo spectra of the highly mobile component of sample PA(5). Echo times were 4 ms for the ^{1}H and 2 ms for the ^{13}C experiments, respectively.

Therefore, the fraction of the γ-crystalline phase reveals the gradual increase at a clay content above 2.5 wt %. Apart from the clay polymer interaction also flow-induced chain elongation in the presence of clay platelets largely enhances the formation of the γ-crystalline phase.

3.4. Mobility of Nylon Chains and Organic Clay Modifier−Identification of the Highly Mobile Component. In an investigation of a similar nylon 6−montmorillonite system, Vanderhart observed a highly mobile component in the ^{1}H spectra[19] and assigned it to the organic modifier that decomposed to a tertiary amine. On the basis of the relative intensities of the different chemical shifts he proposed that a methyl group was abstracted from the quaternary ammonium ion. We observed as well a highly mobile component in our system. The fraction of this mobile component as a function of clay content is shown in Figure 5.

At clay contents higher than or equal to 5 wt %, about 25−40% of the total surfactant has decomposed. For lower clay contents the fraction of decomposed surfactant is less than 10% which indicates that decomposition is stronger at higher clay contents. But it has to be pointed out that the determination of the very small amounts of the highly mobile compound in the ^{1}H spectrum is less accurate for lower amounts of clay. Another reason for the lower amount of decomposed surfactant at lower clay content could be evaporation of the decomposition product at the end of the extruder or removal by escaping water. This could be more probable for small clay contents because the clay layers act as barriers hindering mass diffusion.

To get more detailed information about the chemical origin of the highly mobile component and to test if the same decomposition product is generated as seen in refs 20 and 25, additional ^{1}H and ^{13}C NMR measurements were performed. For both nuclei, NMR spectra were recorded using a rotor-synchronized Hahn echo experiment. The resulting

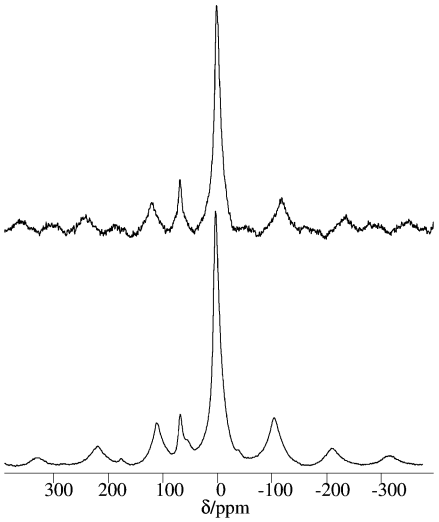

Figure 7. ^{27}Al spectra of pure clay (top) and of sample PA(20) (bottom).

spectra are shown in Figure 6 for the ^{1}H (top) and ^{13}C spectra (bottom) of sample PA(5). In the ^{1}H spectrum, three resonances can be distinguished: The major signal at 1.3 ppm together with a less intense signal at 0.9 and a broader signal with two peaks around 2.2 ppm. The ^{13}C spectrum shows multiple resonances with the major signal at 30.6 ppm and other resonances at 58.6, 32.7, 28.3, 23.4, and 14.7 ppm together with a signal of small intensity at 42.4 ppm indicated by the arrow in Figure 6. From databases,[55,56] a clear assignment of this highly mobile component is possible. It does not originate from nylon 6, since nylon 6 chain fragments show ^{1}H resonances at 3.3 ppm and ^{13}C resonances at 39, 36, and 25 ppm apart from the carbonyl resonance that might be absent due to the short recycle delay. Another possibility is that caprolactam might be formed during

(55) Pouch, C. J.; J. Behnke, E. *Aldrich Library of ^{13}C and ^{1}H FT NMR Spectra*; Aldrich: Milwaukee, WI, 1993.
(56) http://www.aist.go.jp/RIODB/SDBS/menu-e.html (accessed Oct 2006).

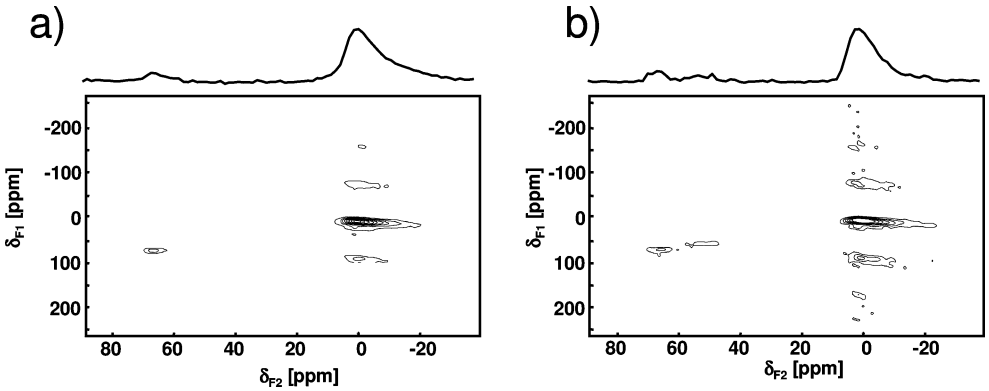

Figure 8. 2D MQMAS spectrum of (a) pure clay and (b) sample PA(20).

processing which has signals similar to those of nylon 6. The organic modifier, dimethyl di(hydrogenated tallow) ammonium which shows a proton resonance around 3.4 ppm and carbon resonances around 53 and 66 ppm, can also be excluded. With the ^{13}C chemical shifts, a clear assignment can be done. A tertiary amine with two methyl groups leads to signals at 45.5 for the methyl groups and 60.1 ppm for the carbon of the hydrogenated tallow next to the nitrogen atom, whereas the amine with only one methyl group has resonances of 42.4 and 58.1 ppm, which much better coincide with the observed resonances. The other resonances of the tallow carbons are identical for both structures. Proton and carbon resonances for the tertiary amine are summarized in Scheme 1.

A combination of high temperature and mechanical mixing leads to a decomposition of the organic modifier.[20,25] Furthermore, the small line width makes it likely that it is remote from the clay surface. Otherwise, the paramagnetic Fe^{3+} would produce a broadening of the lines.

3.5. Structure of Montmorillonite Clay and Its Interactions with the Polymer Matrix. The results so far show the influences of the clay on the polymer. To investigate the opposite, that is, modifications of the clay structure due to the presence of nylon 6, we compared the ^{27}Al spectra of the pure clay and the nanocomposite.

^{27}Al is a favorable nucleus for NMR and has a high natural abundance, and because it is a quadrupolar nucleus, the symmetry of the surroundings is reflected by the quadrupolar coupling. So far, the use of ^{27}Al NMR for the characterization of polymer−clay nanocomposites has been limited.[52,57] Only the changes in line width between pure clay and the nanocomposite were discussed.

Montmorillonite is a 2:1 phyllosilicate consisting of a middle layer of six-coordinated aluminum which is surrounded by two layers of four-coordinated silicon, and oxygen interconnects aluminum and silicon. To some degree silicon is replaced by four-coordinated aluminum in the outer layer, thereby creating a negative charge in these silicates. Additionally, replacement of aluminum by magnesium in the octahedral environments creates a negative charge as well. This overall negative charge is counterbalanced mainly by sodium cations that are placed between the three-layer sheets.

Table 3. Isotropic Chemical Shift and SOQE Values from MQMAS Measurements[a]

sample	coordination site	δ_{iso} [ppm]	SOQE [MHz]
pure clay	$AlO_{6/3}$	4.9	3.8
	$AlO_{4/2}$	70.6	3.6
PA(20)	$AlO_{6/3}$	6.8	4.1
	$AlO_{4/2}$	71.5	3.9
	$AlO_{4/2}$	58.2	3.6

[a] Uncertainties are 10%.

In our case, the sodium cations have been largely ion-exchanged by quaternary ammonium ions.

The ^{27}Al spectrum of pure clay is shown in the top of Figure 7. The most intense signal with a chemical shift around 0 ppm stems from the six-coordinated aluminum sites, and a smaller signal at 67 ppm is from the four-coordinated aluminum sites at the clay surface.[58−60] Other signals are part of the many spinning sidebands due to the second-order quadrupolar broadening. The corresponding spectrum of sample PA(20) is also included in Figure 7, bottom. In addition to the two signals from the pure clay, a small signal exists as a shoulder at about 50 ppm. From its position it probably originates from a second four-coordinated aluminum site.

A more detailed analysis and better separation of individual signals is possible with the 2D MQMAS experiment.[33,37] The 2D spectra of the pure clay (a) and sample PA(20) (b) are compared in Figure 8. The additional signal is only observed in the nanocomposite and clearly separated from the other signals. Therefore, this additional signal is the result of the nanoscopic structure of the material. The determined values for the isotropic chemical shift, without the quadrupolar induced shift, and the SOQE of the ^{27}Al resonances are summarized in Table 3. The isotropic chemical shift of 58.2 ppm for the additional signal clearly corresponds to a four-coordinated aluminum site. This means that the surface layer of the clay sheets is modified, preferably by the adjacent polymer chains. A more detailed analysis of the interactions of polymer and clay could be possible with ^{15}N $\{^{27}Al\}$ REAPDOR[61] or TRAPDOR[62] measurements but would

(57) Nogueira, R. F.; Tavares, M. I. B.; Gil, R. A. S. S. *J. Metastable Nanocryst. Mater.* **2004**, *22*, 71−75.
(58) Goodmann, B. A.; Stucki, J. W. *Clay Miner.* **1984**, *19*, 663−667.
(59) Komarneni, S.; Roy, R.; Fyfe, C. A.; Kennedy, G. J.; Strobl, H. *J. Am. Ceram. Soc.* **1986**, *69* (3), C−42−4.
(60) Guo, J.; Li, L.; Yuan, H.; Yang, N.; Wang, D.; Chen, F. *Chin. Sci. Bull.* **1995**, *40*, 1007−1011.
(61) Holland, G. P.; Alam, T. M. *Phys. Chem. Chem. Phys.* **2005**, *7*, 1739−1742.

require isotopic labeling which is far outside the scope of this paper.

Similar SOQE values for the individual aluminum sites of the pure clay and the PA(20) nanocomposite indicate that no dramatic changes to the clay structure took place. The quadrupolar coupling is slightly higher for the nanocomposite which indicates a lower symmetry of the aluminum surrounding. The additional site in the nanocomposite also has a SOQE value similar to that of the other four-coordinated aluminum site.

These results reveal that not only the clay has an influence on the polymer but also vice versa. However, this additional aluminum site was observed in the sample with the highest clay content. Unfortunately, samples with lower clay content are more difficult to analyze because of their low clay and, therefore, aluminum content. Improvements could be possible by enhancement techniques such as DFS (double frequency sweeps).[63,64] Work along this line is in progress.

4. Conclusions

The application of different solid-state NMR spectroscopic techniques to nylon 6−montmorillonite nanocomposites was demonstrated to yield detailed molecular structure information. Apart from other studies which have been performed for nanocomposites with a maximum clay content of 5%, the samples investigated here show very good exfoliation even at high clay loadings of 20 wt %. From ^{15}N CPMAS NMR spectra an increase of the fraction of the γ-crystalline phase of nylon 6 was observed at the cost of the α-crystalline phase. This preferable formation of the γ-crystalline phase due to the presence of clay platelets is in agreement with previous investigations that have explored the different T_1 relaxation behaviors of the two phases.[19,54] The influence of the paramagnetic Fe^{3+} ions in the clay on the ^{1}H T_1 relaxation time of the polymer was observed and, on the basis of the surface-to-volume ratio of the clay, used to deduce information about the degree of clay exfoliation.

For the first time, a detailed look to the clay structure was performed by studying the ^{27}Al nucleus. With the 2D MQMAS experiment an additional four-coordinated site was found in the nanocomposite that is probably formed as a result of a surface modification of the clay because of interaction with the polymer matrix. Furthermore, it was possible to assign the chemical structure of highly mobile molecules that are formed during the extrusion process. These molecules are the organic modifier dimethyl di(hydrogenated tallow) ammonium ion that lost a methyl group upon compounding. This decomposition was also observed in a similar system,[20,25] but with the highly resolved ^{13}C spectrum, the complete spectroscopic assignment was possible.

These results demonstrate that various types of information can be obtained by solid-state NMR spectroscopy. Both the organic and the inorganic components can be studied. Therefore, solid-state NMR spectroscopy is a valuable tool of analysis for obtaining morphological information about this class of materials. Further investigations will deal with the characterization of clay structures in nanocomposites with lower clay content and the chemical reactions taking place during the extrusion process in nanocomposites with different organic modifiers.

CM052798X

(62) Holland, G. P.; Cherry, B. R.; Alam, T. M. *J. Phys. Chem. B* **2004**, *108*, 16420−16426.
(63) Haase, J.; Conradi, M. S. *Chem. Phys. Lett.* **1993**, *209*, 287−291.
(64) Iuga, D.; Schäfer, H.; Verhagen, R.; Kentgens, A. P. M. *J. Magn. Reson.* **2000**, *147*, 192−209.